A HIGH-RESOLUTION 21-CM HYDROGEN-LINE SURVEY OF THE ANDROMEDA NEBULA

MORTON S. ROBERTS
National Radio Astronomy Observatory,* Charlottesville, Virginia
Received October 6, 1965

ABSTRACT

A survey of 21-cm hydrogen-line radiation was made over the central 2° of the Andromeda Nebula (M31). The observations were obtained with a 20-channel receiver and the 300-foot radio telescope; at 21 cm the beam width of this telescope is 10′, which corresponds to 2 kpc at the distance of M31. Among the results derived are: a map of the radial-velocity field, the rotation-curve, the total mass, and the distribution of the integrated brightness temperature. The radial-velocity map for M31 displays a striking diagonal symmetry—one pair of quadrants agrees quite well with predictions from a model based on a thin disk in pure rotation, while the other pair is in marked disagreement with such a model. An over-all expansion or contraction on a galactic scale cannot explain these features. The most direct explanation of the complex regions is in terms of bends at the ends of the hydrogen distribution similar to those found in our own Galaxy. The positions of loci of constant radial velocity near the minor axis require an additional mechanism for their explanation; a combination of expansion *and* contraction over various parts of M31 appears necessary.

A rotation-curve was derived from data points in the "ordered" quadrants. The two halves of this rotation-curve are not symmetrical; this has been noted previously by Burke, Turner, and Tuve. The average total mass derived from the two quadrants as well as the mass computed from the combined (reflected) data is $3.1 \times 10^{11}\ \mathfrak{M}\odot$. The systemic radial velocity derived from the rotation-curve is −310 km/sec. A comparison is made between Mayall's optically derived radial velocities and the 21-cm data. There is qualitative agreement between his measures and the complex-region data. Over the region common to the present study, his measures are of emission regions confined exclusively to the complex regions.

The integrated hydrogen distribution shows a clear ringlike shape of 10 kpc radius with a distinct minimum in the central regions of Andromeda. A comparison between the locations of the peak H I ridge line and the distribution of emission nebulae mapped by Baade and Arp shows good general agreement. The H I distribution is, however, shifted west by ∼1′ with respect to the concentrations of H II regions. This displacement could be attributed to uncertainties in the 300-foot telescope pointing corrections only by invoking the combined maximum errors in right ascension and declination. There is thus a high probability that there is a displacement in the plane of up to 1 kpc between the optical spiral features and the location of the peak hydrogen concentrations.

I. INTRODUCTION

Of the galaxies visible in the northern sky, the Andromeda Nebula (M31 = NGC 224) is the system of largest angular extent and is thus ideal for 21-cm hydrogen-line studies. The results of such a study, made with the 300-foot meridian telescope of the National Radio Astronomy Observatory, are presented here. The results include a map of the radial-velocity field, a rotation-curve from which has been derived a total mass, and contours of the distribution of 21-cm line radiation over the central regions of M31. These data have been derived with an antenna whose beam pattern is circular and has a total width at half-intensity of 10′. At the distance of M31, 0.69 Mpc (Baade and Swope 1963), 10′ corresponds to 2.0 kpc.

Previous studies of Andromeda have been made by van de Hulst, Raimond, and van Woerden (1957), Argyle (1965), Brundage and Kraus (1965), and by Burke, Turner, and Tuve (1963, 1964*a*, *b*; hereinafter referred to as "BTT"). The antenna beam sizes used in these studies were 34′, 36′, 10′ × 38′, and 10′, respectively. The BTT observations, also made with the 300-foot telescope, were of selected points along the major and minor axes of M31. They derived the run of projected density along the major axis and a rotation-curve. Of especial interest is their finding of different rotation-curves for the NF and SP sections of Andromeda; this result is confirmed in the present study.

* Operated by Associated Universities, Inc., under contract with the National Science Foundation.

II. OBSERVATIONS

The observations discussed here were obtained during two observing periods, one in 1963 and the other in 1964, and were made with a 20-channel receiver. Each channel is 95 kHz = 20 km/sec wide at the 3-db points and is approximately rectangular in shape; the filter centers are spaced by 100 kHz ≈ 21 km/sec. The details of the receiver, which had an over-all system-noise temperature of 250° K, have been described previously (Höglund and Roberts 1965). The signal-to-noise ratio was such that one observation at each of the chosen declinations was adequate for reduction purposes. At some declinations two observations were made and averaged together. In addition, several declinations were common to both observing periods to insure a proper tie-in of the data; a log of the observations is given in Table 1. A declination range 60′ north to 50′ south of the optical center was measured; however, the 2 MHz = 420 km/sec range of the filters was not adequate to cover the radial-velocity range of the galaxy and the integrated hydrogen data can only be considered complete to 30′ either side of the center. For those

TABLE 1

SUMMARY OF OBSERVATIONS

Observing Period*	No of Drift-Curves	Declination Offset from Center	Observing Period*	No. of Drift-Curves	Declination Offset from Center
A	1	60′.5 N.	B	1	4′.5 S.
A	1	50.5 N.	A	1	9.5 S.
A	1	40 5 N.	B	1	14 5 S.
A, B	1, 2	30.5 N.	A, B	1, 2	19.5 S.
A	1	25 5 N.	A	2	23 5 S.
A, B	1, 2	20.5 N.	A, B	1, 2	29.5 S.
A	1	10 5 N.	A	1	39.5 S.
B	1	5 5 N.	A	1	49.5 S.
A, B	2, 2	0 5 N.			

* A, September, 1963; B, July, 1964.

declinations observed during the second period the central frequency of the filter bank was shifted to allow for the over-all velocity range. Observations were spaced at most 10′ apart in declination and in several cases 5′; in addition, measurements were made at the declinations of NGC 205 (25′ north of the center) and M32 (24′ south). The basic data tapes were reduced at the Harvard University Computing Center and at the computing facilities of the Institute for Space Studies.

These observations differ from the previous 25-m telescope studies in that the filter width is narrower, i.e., the velocity resolution is greater, and the angular resolving power is more than three times greater. It also differs from the BTT (1963, 1964*a*, *b*) 300-foot study in that over the declination range in common these data refer to the full galaxy rather than to points along the major and minor axes; however, the filter widths are significantly wider than in the BTT study. The full coverage in right ascension yields a surprising and completely unexpected radial-velocity map which will be discussed below.

A reproduction of the analogue record for six velocity channels of an observation taken close to the center (0′.5 north) is shown in Figure 1. The velocities in this figure and throughout this paper are with respect to Sun; to convert these velocities to the local standard of rest add +4 km/sec. The second and third drift-curves in Figure 1 bracket the systemic radial velocity of Andromeda and therefore refer to regions close to or at the center. It can be seen that the antenna temperature is a minimum at the right ascension of the center, and an extensive, high H I content in the central regions must be ruled out.

This is also evident in the hydrogen contours of BTT (1964*a*). The previously reported (van de Hulst *et al.* 1957) picture of a high projected density of neutral hydrogen in the center of M31 has also been altered by van Woerden (see Oort 1965).

The peak antenna temperatures displayed in the drift-curves in Figure 1 range from 1° to 10° K. The highest antenna temperature measured in this survey is 12° K, which, with a beam efficiency of 53 per cent, corresponds to a peak brightness temperature of ~24° K.

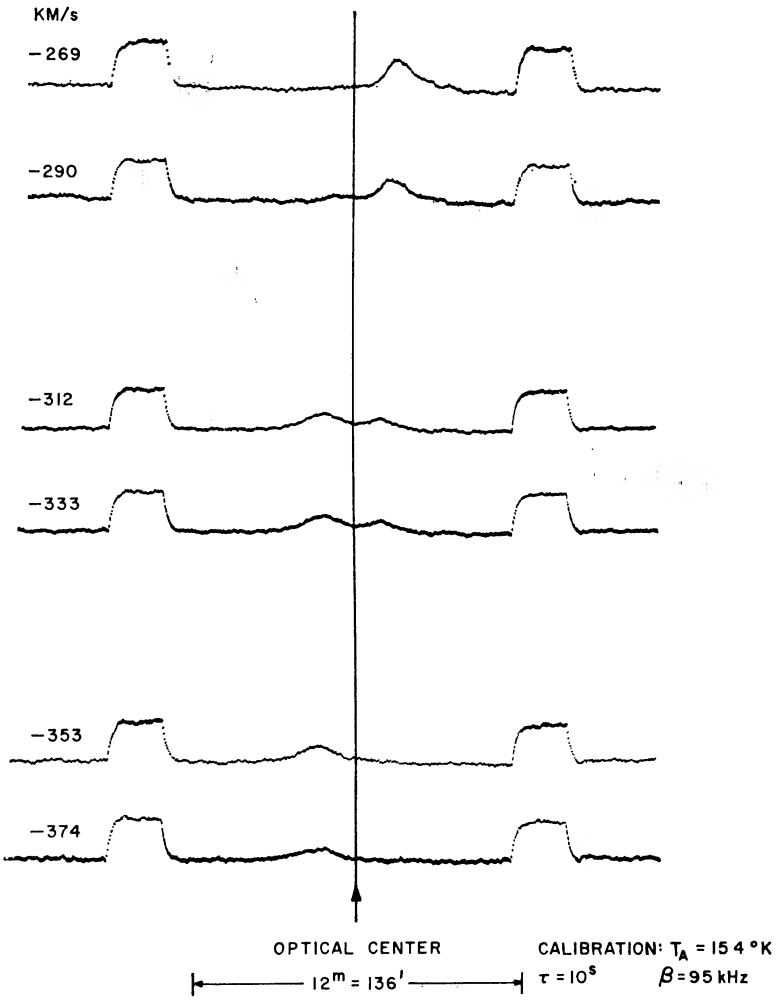

FIG. 1.—The analogue display of drift-curves for 6 of the 20 channels. The declination is 0.5 north of the center. The central vertical line marks the optical center.

III. RESULTS

a) Radial-Velocity Field

We are here interested in the over-all motion within M31 and may think of the 21-cm radiation as a probe for studying the radial-velocity field. The observational data are a series of drift-curves, right ascension versus antenna temperature, at a variety of declinations and velocities from which we can construct, as a first step, a map of the radial-velocity field. Such a map will display the loci of constant radial velocity as seen on the projected image of Andromeda. The spatial coordinates of a point on such a plane are

fixed by the declination setting of the telescope and a measure of right ascension derived from the drift-curve display of a signal. In the following, all positions in right ascension, α_i, refer to the location(s) of the peak(s) of a drift-curve made at declination δ_i and velocity v_i. Other measures of position that may be used are the mean ($\Sigma T_j \alpha_j / \Sigma T_j$) and the median of a drift-curve signal. These two measures involve a weighting by the hydrogen distribution while the peak position minimizes, as much as possible, the influence of the hydrogen distribution on the derived velocity map. All three methods yield the same position when the drift-curve signal is symmetrical. The values (α_i, δ_i, v_i) for all measured peaks are listed in Table 2.

A standard error of $5^s \approx 1'$ for an individual measurement was derived from repeated measures of α_i and from comparison between eye estimates of α_i and a computer-derived fit of a Gaussian curve to those signals having a symmetric shape. An intercomparison of the measured α_i for data common to the two observing periods gave a standard error of 7^s; this value is just that expected from measurement errors in the two sets of data, and we may safely say that there is little or no systematic difference between the two observing periods.

Some of the drift-curves are quite asymmetric or have low flat shapes. In a weighting scale of 1–4 based on the confidence in the measured α_i, these were given weight 1 and were not used in the determination of the rotation-curve for Andromeda or in deriving the standard errors discussed above. They are, however, plotted, along with the higher weight points, in Figure 2 which displays the observed loci of constant radial velocity for M31. In this figure the individual pairs (α_i, δ_i) of a common v_i have been connected with straight lines; a dashed line is used when the points connected are farther apart than $10'$. Some of the data do not have velocities in common with the majority of the material and would therefore have been represented as single points. For clarity of the diagram, these have not been plotted in Figure 2 but were used in the rotation-curve solution. Where possible, averages of α_i's for δ_i and v_i common to the two observing periods were used. To further improve the clarity of the diagram, numbers from -1 through $+20$ were used to identify the radial velocities rather than the actual values. The velocity step is ~ -21 km/sec with -1 corresponding to ~ -58 km/sec, e.g., 0 is ~ -79 km/sec, 5 is -184 km/sec, etc. Beyond $\pm 30'$ (in declination) from the center, the map may be incomplete if the radial velocity of that part of M31 lay outside the velocity range of the total band width employed. Within this central region, the absence of a velocity point at a particular declination indicates too low a signal-to-noise ratio for measurement.

The striking feature in the observed radial-velocity field is the diagonal symmetry displayed by the loci. One pair of quadrants have their loci rather evenly spaced while the other pair have an irregular ordering of the loci. The crowding together of the loci in these regions indicates that at a given point along the line-of-sight there is a large spread in the radial velocity.

For comparison with the observed loci diagram, we present in Figure 3 the expected appearance of such a diagram for a system displaying pure circular motion and having the inclination and rotational parameters of M31. The lines in this figure cover a range $\pm 70'$ along the major axes and are spaced by 20 km/sec, the approximate spacing of the velocity filters used in this study. Any given filter, v_i, can only receive radiation from the galaxy from a region defined by these lines. If the filter width is $v_i \pm 10$ km/sec and if there is an average random motion of the hydrogen of 10 km/sec with respect to the appropriate regional standard of rest, then the emitting region that can be sensed by filter v_i is centered on line v_i and has a width of $\sim \pm 20$ km/sec, or the spacing of the loci in Figure 3. If radiation at velocity v_i is found outside this "permitted" region, we may question the assumptions made in constructing Figure 3, namely: (1) circular motions only; (2) the size and extent of the random motions; (3) the inclination; and (4) the flatness of the emitting system, i.e., do extensive regions of the H I distribution define another inclination angle?

TABLE 2

MEASURES FROM DRIFT-CURVES

Radial Velocity (km/sec)	1950 α 00^h+	Declination from Center	Weight	Radial Velocity (km/sec)	1950 α 00^h+	Declination from Center	Weight
−56 1	42^m20^s	+30′5	2	−198 5	40^m43^s	+25′5	4
	42 55	+20 5	1	−203 1	40 25	+20 5	3
	41 43	+20 5	1		42 11	+20 5	2
−72 0	42 02	+25 5	2		44 23	+20 5	1
−77 0	42 34	+30 5	3	−205 8	41 30	+60 5	2
	41 38	+20.5	2		41 02	+50 5	2
	43 18	+20 5	1		40 54	+40 5	4
−93 1	42 42	+25 5	4		40 48	+30 5	2
−98 3	42 45	+30 5	4		40 30	+20 5	4
	41 15	+20 5	2		42 09	+20 5	1
−99 4	41 56	+40 5	2		42 06	+10 5	3
	43 28	+40 5	1	−206 1	41 58	+ 0 5	1
	42 52	+30 5	4	−218 2	40 26	+25 5	4
	41 48	+30 5	1		44 04	+25 5	3
	41 29	+20 5	2	−224 5	40 20	+30 5	3
	42 35	+20 5	2		40 18	+20 5	4
−114 0	42 39	+25 5	4	−226 8	40 58	+50 5	1
−119 3	42 57	+30 5	4		40 34	+40 5	2
	42 33	+20 5	3		40 27	+30 5	3
−121 4	41 53	+40 5	4		40 19	+20 5	4
	43 38	+40 5	1		43 43	+20 5	1
	43 00	+30 5	3		42 09	+20 5	1
	41 45	+30 5	1		41 56	+10 5	4
	42 30	+20 5	4		43 38	+10 5	1
−135 2	42 37	+25 5	3		41 44	+ 0 5	4
−139 9	41 30	+30 5	2		41 39	+ 0 5	3
	43 00	+30 5	2	−227 0	41 41	+ 0 5	4
	42 28	+20 5	4	−239 8	40 05	+25 5	4
−142 5	41 46	+40 5	4	−269 4	39 55	+30 5	3
	41 29	+30 5	4	−246 5	40 02	+20 5	4
	43 01	+30 5	4	−415 7	39 22	−29 5	4
	42 30	+20 5	4		36 30	−29 5	2
−150 4	41 23	+30 5	2		39 09	−39 5	2
	42 57	+30 5	2		38 30	−49 5	1
	42 28	+20 5	4	−417 0	38 35	+ 0 5	2
−156 4	42 43	+25 5	4	−417 3	38 40	− 4 5	3
−161 5	41 05	+30 5	3	−421 6	39 33	−19 5	3
	42 41	+30 5	2		37 18	−19 5	4
	42 26	+20 5	4	−427 1	39 15	−29 5	2
−163 4	42 29	+60 5	3		36 56	−29 5	2
	41 27	+40 5	4	−436 8	38 28	− 9 5	3
	44 45	+40 5	1		39 25	−19 5	3
	41 12	+30 5	3		37 12	−19 5	3
	42 55	+30 5	1		39 17	−23 5	3
	42 31	+20 5	4		37 06	−23 5	4
	41 03	+20 5	1		38 59	−29 5	3
	42 15	+10 5	1		36 53	−29 5	4
−177 4	40 54	+25 5	4		38 47	−39 5	4
	42 44	+25 5	2	−437 1	39 45	−14 5	2
−182 6	41 00	+30 5	3	−438 1	38 35	− 4 5	3
	42 22	+20 5	4	−442 7	39 32	−19 5	4
−184 6	41 52	+60 5	2		37 04	−19 5	2
	45 23	+60 5	1	−448 4	38 55	−29 5	4
	41 39	+50 5	3		36 55	−29 5	3
	41 14	+40 5	4	−456 8	38 24	− 9 5	3
	40 55	+30 5	4		37 30	−19 5	2
	44 25	+30 5	1		39 13	−19 5	1
	42 28	+20 5	3		36 53	−23 5	4
	40 50	+20 5	1		39 07	−23 5	1
	42 03	+10 5	3		38 50	−29 5	3

TABLE 2—*Continued*

Radial Velocity (km/sec)	1950 α 00h+	Declination from Center	Weight	Radial Velocity (km/sec)	1950 α 00h+	Declination from Center	Weight
−456 8	36m49s	−29′5	4	−310 3	39m03s	+10′5	4
	38 35	−39 5	4		38 59	+ 0 5	3
−463 2	39 25	−19 5	3		40 58	+ 0 5	4
	37 45	−19 5	3		40 55	+ 0 5	3
−469 4	38 55	−29 5	2		38 56	+ 0 5	2
	36 47	−29 5	4		40 57	− 9 5	4
−478 1	38 09	− 9 5	1		41 13	−19 5	3
	37 55	−19 5	3		38 39	−19 5	1
	39 05	−19 5	1		41 14	−23 5	2
	37 42	−23 5	2		41 14	−29 5	2
	39 06	−23 5	1	−310 9	40 56	−14 5	2
	36 29	−29 5	3		42 06	−14 5	1
	38 40	−29 5	1	−311 5	40 50	+ 0 5	4
	38 12	−39 5	3		38 50	+ 0 5	4
	36 11	−39 5	2	−311 8	40 50	− 4 5	4
−484 6	37 55	−19 5	3		39 05	− 4 5	1
−490 0	38 29	−29 5	2	−312 1	38 59	+ 5 5	3
−499 3	37 56	−19 5	2	−316 2	41 04	−19 5	3
−247 9	40 23	+40 5	2	−321 9	40 59	−29 5	2
	40 01	+30 5	4	−331 5	39 05	+10 5	3
	40 03	+20 5	4		38 41	+ 0 5	3
	40 00	+10 5	3		38 36	+ 0 5	3
	43 59	+10 5	2		40 34	+ 0 5	1
	41 45	+10 5	3		40 30	+ 0 5	1
	41 34	+ 0 5	3		40 37	− 9 5	4
	41 33	+ 0 5	3		38 32	− 9 5	1
−248 3	41 40	+ 0 5	4		40 48	−19 5	3
−248 6	41 46	− 4 5	1		38 05	−19 5	2
−260 9	39 37	+25 5	4		40 51	−23 5	3
−267 0	39 42	+30 5	3		40 48	−29 5	2
	39 56	+20 5	4	−332 6	38 46	+ 0 5	4
−267 6	39 37	+30 5	2		40 49	+ 0 5	3
	39 40	+20 5	3	−332 9	38 28	− 4 5	3
	39 45	+10 5	2		40 41	− 4 5	3
	43 14	+10 5	1	−333 2	38 55	+ 5 5	3
	41 27	+10 5	1	−337 1	40 34	−19 5	4
	41 21	+ 0 5	4	−343 2	40 40	−29 5	3
	41 23	+ 0 5	3	−352 5	40 28	−14 5	4
	39 40	+ 0 5	1	−352 8	38 31	+ 0 5	4
	41 15	− 9 5	2		38 23	+ 0 5	3
−268 7	42 26	−14 5	1		38 58	+ 0 5	1
−269 3	41 25	+ 0 5	4		40 25	− 9 5	4
−269 6	41 29	− 4 5	2		37 46	− 9 5	2
−282 1	39 18	+25 5	2		40 21	−19 5	4
−287 8	39 25	+30 5	2		37 55	−19 5	1
	39 16	+20 5	4		40 19	−23 5	2
−289 2	39 04	+20 5	2		37 42	−23 5	1
	39 20	+10 5	4		40 05	−29 5	2
	41 15	+ 0 5	4		39 51	−39 5	3
	41 09	+ 0 5	2	−353 1	38 32	+ 0 5	2
	39 29	+ 0 5	1		41 26	+ 0 5	1
	41 09	− 9 5	3	−353 4	38 20	− 4 5	4
	41 39	−19 5	1		40 29	− 4 5	2
	42 04	−23 5	2	−354 5	38 40	+ 5 5	2
−289 9	41 11	+ 0 5	3	−358 4	40 13	−19 5	3
−290 2	39 24	− 4 5	2	−363 0	40 27	−14 5	4
	41 10	− 4 5	4	−372 7	38 43	+ 0 5	2
−295 0	41 52	−19 5	2		38 49	+ 0 5	2
−300 4	41 04	+ 0 5	3		40 09	− 9 5	3
−300 7	41 04	− 4 5	4		37 55	− 9 5	3
−308 5	38 55	+20 5	1		40 09	−19 5	4

TABLE 2—*Continued*

Radial Velocity (km/sec)	1950 α 00h+	Declination from Center	Weight	Radial Velocity (km/sec)	1950 α 00h+	Declination from Center	Weight
−372 7	37m09s	−19′5	2	−400 0	39m45s	−19′5	3
	39 55	−23 5	4	−406 2	39 23	−29 5	3
	37 25	−23 5	1	−410 5	39 40	−19 5	2
	40 00	−29 5	3		37 25	−19 5	3
	39 37	−39 5	2	−415 7	38 38	+ 0 5	3
	39 25	−49 5	1		38 29	− 9 5	3
−374 5	38 40	+ 0 5	2		37 31	− 9 5	1
−374 8	38 13	− 4 5	3		39 35	−19 5	4
	40 15	− 4 5	3		37 18	−19 5	4
−379 4	40 04	−19 5	4		39 27	−23 5	4
	37 10	−19 5	2		37 13	−23 5	4
−385 0	39 50	−29 5	2	−499 3	38 01	−23 5	2
−394 7	38 43	+ 0 5	3		38 29	−29 5	2
	38 45	+ 0 5	3		36 33	−29 5	1
	37 45	− 9 5	3		38 09	−39 5	2
	40 03	− 9 5	1		36 33	−39 5	4
	39 52	−19 5	4		37 43	−49 5	3
	37 16	−19 5	2		35 59	−49 5	1
	39 44	−23 5	4	−500 5	38 20	−29 5	2
	36 51	−23 5	3	−506 5	37 57	−19 5	2
	39 48	−29 5	3	−511 6	38 18	−29 5	2
	36 40	−29 5	2	−527 1	38 11	−19 5	2
	39 37	−39 5	1	−532 7	38 06	−29 5	3
	38 58	−49 5	3	−547 9	38 08	−19 5	4
−395 2	39 57	−14 5	3	−553 2	37 51	−29 5	4
−396 7	38 32	− 4 5	2	−574 6	37 50	−29 5	4
	40 20	− 4 5	1				

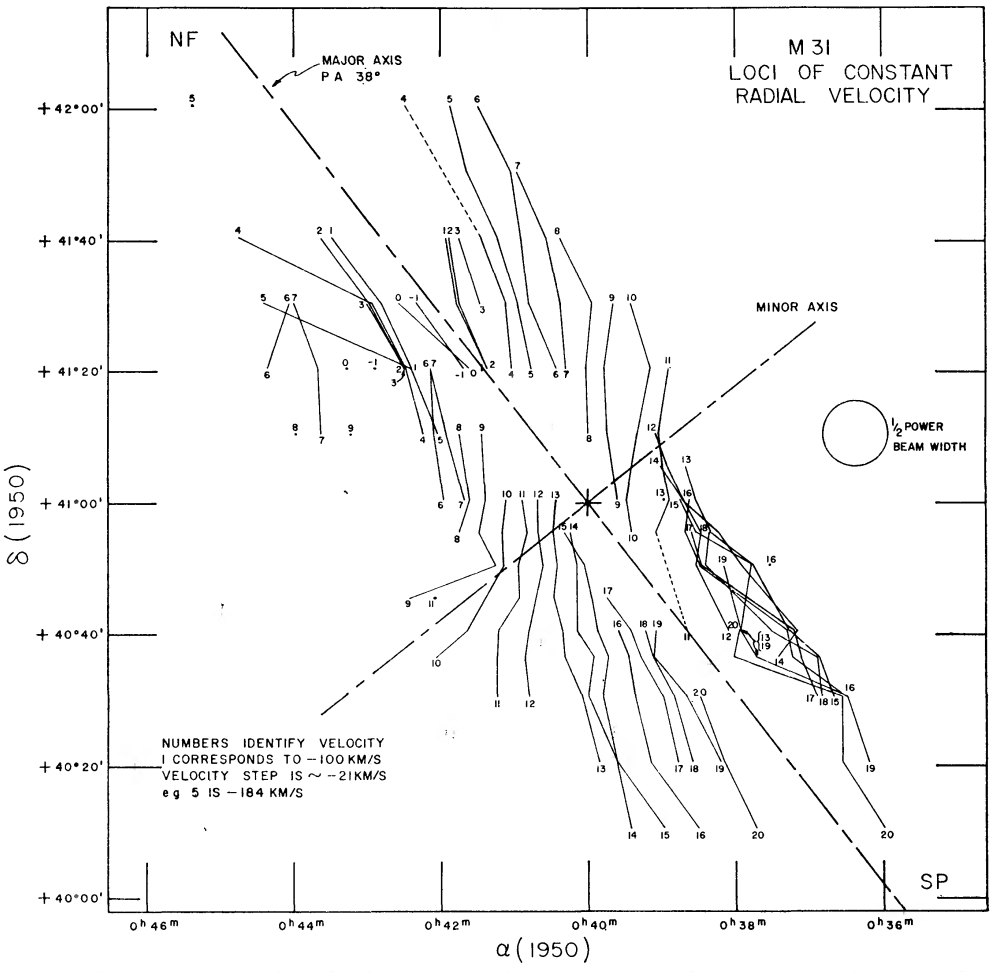

FIG. 2.—A map of the observed radial-velocity field for M31. See Fig. 3 for a theoretically derived map.

The observed loci of Figure 2 show good agreement with the expected loci of Figure 3 in only two quadrants: the preceding section of the north part of the galaxy and the following side of the south end. We shall refer to these regions as the "ordered" quadrants. The other two qudrants greatly deviate from the expected spacing of the loci, and we shall call these the "complex" quadrants. The division by quadrants is one of convenience since even along the minor axis where we expect a single straight line for the locus, that of the systemic radial velocity, we find serious disagreement between the

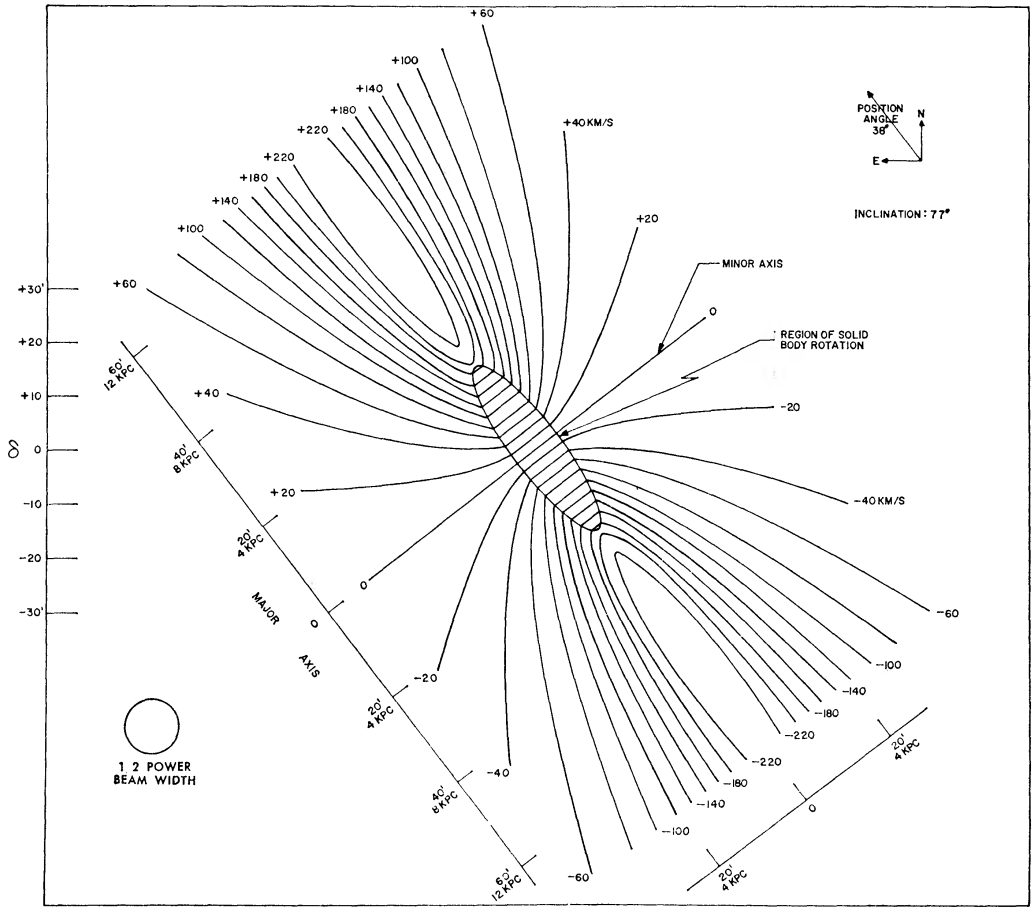

FIG. 3.—A map of the loci of constant radial computed for a thin disk, pure rotational model

observed and predicted loci. It should be noted that the crossing of the loci of constant radial velocity is merely due to our method of constructing Figure 2; the resolving power is not great enough to construct the more appropriate "isovels."

The possibility that measurement errors and the uncertainty in declination due to antenna-beam size are responsible for the appearance of the complex regions was tested in the following way. A radial-velocity map was constructed where each data point was inclosed in an error box; the various loci were then drawn using any part of this error box rather than the central data point in an attempt to obtain the symmetry of Figure 3. It quickly became evident that such a procedure could not improve the general appearance of the complex quadrants and that some physical cause in M31 is responsible for the over-all features of Figure 2. As can be seen from Figure 1, many of the paired points of a common radial velocity and declination come from the same drift-curve, and yet one point lies in the ordered region and the other in the complex region. It is thus difficult to

attribute the appearance of the complex quadrants to instrumental effects. The possible mechanisms responsible for the complex quadrants are implicit in the assumptions adopted in the construction of Figure 3. The effect of relaxing these assumptions will be considered next.

That the complex regions are diagonally opposite as well as the crossing of the minor axis by several loci are suggestive of expansion (or contraction) in addition to the usual rotation. The variation of observed radial velocity with circular velocity along a line whose position angle is ϑ is an even function, $\cos \vartheta$, while the dependence on an expansion velocity is an odd function, $\sin \vartheta$. Thus, going from a purely rotational model to one which has expansion (or contraction) will also alter the loci diagram in a manner which has diagonal symmetry, as is observed. In addition, loci close to the minor axis will be shifted across the minor axis, which is also observed. However, attempts at model fitting showed very poor quantitative agreement with Figure 2. The expansion loci were constructed with the following expression:

$$v = V \sin \xi \cos \vartheta + E \sin \xi \sin \vartheta , \tag{1}$$

where V is the circular velocity at R and ξ is the inclination of the system. Two forms of the expansion term E were used: $E = l/R$ and $E = m/R^2$, where l and m are constants. All the expansion models resulted in loci crossing the minor axes, but values of l as large as 300 km $(\text{sec})^{-1}$ kpc and m as large as 5000 km $(\text{sec})^{-1}$ $(\text{kpc})^2$ gave only minor differences between adjacent quadrants; at $R = 10$ kpc these expansion terms correspond to 30 and 50 km/sec, respectively. Further, although expansion effects cause the loci to cross the minor axis, a detailed comparison between the predictions of simple expansion models and the observed loci were in disagreement. We conclude that expansion is not the principal mechanism responsible for the appearance of the complex quadrants. Because the expected effects of expansion may be masked in some other cause, we cannot argue either for or against a general expansion in M31.

In examining the various other assumptions made in constructing the expected loci diagram of Figure 3 we may, by analogy with our own Galaxy, properly question the assumption of a planar distribution of the emitting hydrogen. In our Galaxy the hydrogen distribution interior to the Sun's position does indeed lie in a very flat plane. However, at distances greater than $R \approx 10$ kpc there is a systematic bending (and flaring out) of the hydrogen; one side of the plane bends up and the other down. At 15 kpc this deviation from the central plane is $\sim$1 kpc (Blaauw and van Woerden, quoted by Robinson 1965; also see Gum, Kerr, and Westerhout 1960). Our Galaxy viewed in 21-cm line radiation from outside would have a varying inclination, the edge-on appearance would be that of an integral sign. Such an effect in M31 would easily explain the complex quadrants. Previous results of optical studies have also encountered the problem of a non-unique inclination angle for Andromeda (de Vaucouleurs 1958; Arp 1964).

That changing the inclination, ξ, of parts of M31 will explain the complex regions can be seen from the effect of ξ on the spacing of the loci of Figure 3. As ξ increases to a more edge-on orientation the loci will become more closely spaced; in the limiting case, when $\xi = 90°$, all the loci will be coincident. Thus, to account for the complex regions by this hypothesis, the direction of bending of the hydrogen distribution on the two sides of M31 must be such as to increase ξ. The loci from the bent regions will become superposed on loci from the principal plane of M31 seen along the same line of sight and result in at least part of the disorder of the complex quadrants. Another contributing factor is the effects of measurement errors, beam smearing, and random motions all of which will appear more exaggerated on the more closely spaced loci of the bent regions. The size of these latter effects may be estimated from the irregularities in the loci of the ordered regions.

It is difficult to estimate quantitatively the maximum inclination necessary to account for the complex regions. Since the loci are not completely coincident we conclude that

$\xi_{max} < 90°$; from model calculations a value of $\xi_{max} \simeq 85°$ appears adequate. If ξ_{max} occurs at 15 kpc, the maximum bend is 8°, twice the value thus far found in our Galaxy. Arp (1964), in an analysis of the distribution of emission nebulae in M31, derives a bend of about the same size, 5°, in the region of the south complex quadrant.

The loci crossing the minor axis can, in part, be attributed to the location of the bent regions seen projected on the sky; at least part of the bends must lie in position angles 128° and 308°. However, this picture will not account for all of the loci crossing the minor axis. The explanation may be improved by having the bends spaced a bit less than 180° apart but some details of the radial-velocity map near the minor axis still require further explanation. It appears that a combination of effects, non-circular but ordered motions and the hydrogen distribution, are needed to account fully for these details of the radial-velocity map. The non-circular motions necessary would have to invoke *both* contraction and expansion as functions of R and ϑ.

The proposal of a non-planar distribution of hydrogen is not a unique explanation of the complex regions, but it has a reasonable foundation in a similar effect in our own Galaxy and in the suggestion of a non-planar distribution of the photographic luminosity for several galaxies including M31.

Other possibilities include a circulation out of the plane of the hydrogen or an *ad hoc* picture of extension and large random motions. The former embraces explanations already considered, while the latter, if strictly gravitational, would require a localized total mass comparable to that of M31. A constraint on any of the explanations is the approximate equality of the mean radial velocity of the receding pair and the approaching pair of quadrants.

Three mechanisms have been proposed for the bending of our own Galaxy: tidal effects due to the Magellanic Clouds (e.g., Burke 1957; Kerr, Hindman, and Carpenter 1957), an intergalactic wind (Kahn and Woltjer 1959), and a precession of the Galaxy due to a difference between the symmetry and angular momentum axes of the Galaxy (Lynden-Bell 1965); each is applicable to M31. The tidal effect would presumably be caused by M32 which may lie quite close to M31 (Schwarzschild 1954). The details of such a mechanism would have to account for the fact that M32 is located near an ordered rather than a complex region. Andromeda's other nearby companion, NGC 205, is also close to an ordered quadrant. The other two arguments are more general. The intergalactic wind explanation requires an intergalactic density of 10^{-4} protons/cm^3; the motion of M31 with respect to the center of mass of the local group would then be in a southeast direction as seen on the plane of the sky. Lynden-Bell's suggestion is perhaps the most attractive and implies that bends in the fundamental plane of a galaxy may be a rather common phenomenon.

b) Rotation-Curve

To construct the rotation-curve, $V(R)$, from data points located at a variety of position angles, we first rotate the measured positions from the equatorial coordinate system to a Cartesian system referred to the center and major axis of M31, and then project the point into the plane of the galaxy. The radial distance of such a point from the center is given by $R = [x^2 + (y \sec \xi)^2]^{1/2}$. For pure circular motions we have a relation between the observed radial velocity and the circular velocity at R similar to equation (1), but less the expansion term:

$$V = (v - s) \csc \xi \sec \vartheta , \tag{2}$$

where $\sec \vartheta = R/x$ and s is the systemic velocity (Höglund and Roberts 1965). The data of Table 2 allow us to make a least-squares solution for $V(R)$; for this we use an interpolation formula of the form

$$V_c = \frac{AR}{[1 + B^n R^n]^{3/2n}} \tag{3}$$

(Brandt 1960). For $n = 3$ we have the Bottlinger-Lohman rotation law (Lohman 1954); for $n = \frac{3}{2}$ we obtain a relation first suggested by Brandt (1960). The constants A and B are determined from the least-squares fit for both the $n = \frac{3}{2}$ and $n = 3$ cases. Through an iterative process we may also determine the coordinates of the rotational center, the systemic velocity, and the position angle of the galaxy. Here, we assume that the best least-squares fit (i.e., the smallest scatter of the residuals) yields the best set of parameters. This procedure will not allow us to determine the inclination because of the complex manner in which it enters the residuals. A value of $\xi = 77°$ was adopted as a compromise value of the several optical determinations.

For each value of n two different determinations of $V(R)$ are made, one in which each half of the rotation-curve is treated separately and the other in which all the data are combined by reflecting the negative points about the origin. In the former case the total rms of the residuals for both solutions is used as a criterion for the fit.

Only the data from the ordered quadrants were used in deriving the rotation-curve, the systemic velocity, and position angle. The coordinates of the rotational center, which were also derived by this method, agree with the optical center to well within the uncertainties in the absolute pointing corrections of the 300-foot telescope which at this declination are 40″ in declination and 3^s in right ascension. Solutions were made both with and without weights; only slight differences were found between these solutions, and the unweighted data were adopted for the final solution.

In addition to the signal-to-noise ratio weighting system, the computer program assigned weights in terms of the value of $\cos \vartheta$ ($\cos \vartheta = 0$ for points on the minor axis) in the following manner: for $\cos \vartheta \leq 0.2$, weight 0, for $0.2 < \cos \vartheta \leq 0.3$, weight $\frac{1}{2}$, and $\cos \vartheta > 0.3$, weight 1. This procedure reduces the effect of uncertainties on V due to uncertainties in positional measurements. Solutions were also made with the weight limits on $\cos \vartheta$ reduced from 0.2 and 0.3 to 0.1 and 0.2, respectively; again only slight differences were found in the final results.

The various solutions—$n = 3$ and $n = \frac{3}{2}$, each half treated separately and data combined, weighted and unweighted—gave values of the position angle from 32° to 41°, with $\frac{3}{4}$ of the values lying in the range 36° to 39°. A value of 38° was adopted which is similar to that used by Baade and Arp (1964) in their discussion of the emission nebulae in M31. The range in the systemic velocity determinations was −306 to −311 km/sec, with $\frac{3}{4}$ of the values lying between −309 and −311. A value of $s = -310 \pm 3$ (est. error) km/sec was adopted.

The derived rotation-curve is shown in Figure 4. The solid line is the least-squares fit of equation (3) to the ordered-quadrants data shown as filled circles in this figure. A value of $n = \frac{3}{2}$, fitted to each half separately, was used. The open circles are points from the complex regions reduced in the same manner. The plus signs are Mayall's (1951) measures of those emission regions which lie in the area of M31 studied here, ±55′ in declination about the center. They too have been treated in the same manner. The comparison of the optical and radio determinations of the rotation-curve will be discussed at the end of this section.

The results of the various solutions described above are summarized in Table 3. The fifth and sixth columns of this table give the locations of the maximum of the rotation-curve, the seventh column lists the rms of the residuals between the data points and the least-squares interpolation equation, while the eighth column gives the total rms for the combined NF and SP solutions. If we adopt equation (3) as representative of the true rotation law, then the total mass is given by

$$\mathfrak{M} = \left(\frac{A}{B}\right)^2 \frac{1}{BG} \tag{4}$$

(Brandt 1960), where G is the gravitational constant; the mass so determined is listed in the ninth column. The mass derived from equation (4) is for a thin-disk model. Brandt

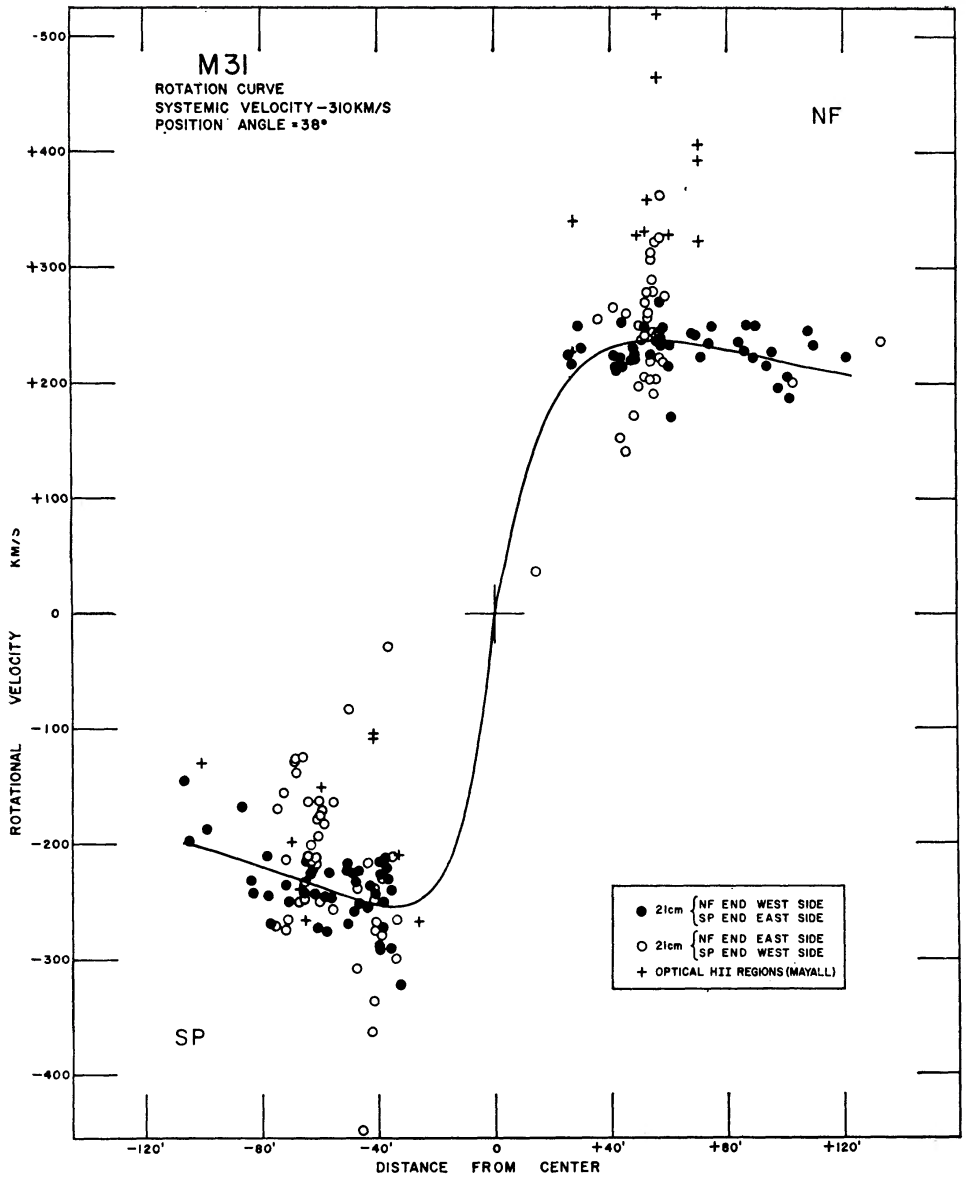

FIG. 4.—Rotation-curve for M31. The solid line is a least-squares fit of eq. (3) to each half of the data. Only the filled circles (from the ordered quadrants) were used in the fit.

TABLE 3

SOLUTIONS FOR ROTATION-CURVE

(Distance = 690 kpc, $s = -310$ km/sec, $\xi = 77°$, Position Angle = 38°, Data Unweighted)

n (1)	Region (2)	A 10^{-15} (sec)$^{-1}$ (3)	B 10^{-23} (cm)$^{-1}$ (4)	V_{max} (km/sec) (5)	R_{max} (kpc) (6)	rms (km/sec) (7)	rms (total) (km/sec) (8)	Mass $10^{11}\odot$ (9)	1 1 Mass $10^{11}\odot$ (10)
3/2	NF	2 11	4 02	238	10 9	18 6	32 1	3 2	3 5
3/2	SP	3 55	7 36	255	7 0	26 2	32 1	2 4	2 6
3 .	NF	1 33	3 95	244	10 3	23 1	35 3	2 1	2 3
3 ..	SP	1 69	4.83	254	8 4	26 7	35 3	1 9	2 1
3/2	Combined	2 67	5 77	244	8 9	24 2	24 2	2 8	3 1
3 ..	Combined	1 51	4 41	250	9 3	25 8	25 8	2 0	2 2

(1960) has shown that a mass increase of 10 per cent will allow for a finite axial ratio of $\sim\frac{1}{10}$; mass estimates including this correction are tabulated in the last column.

The best representation of the rotation-curve for M31 was found for $n = \frac{3}{2}$, though the differences in the fits between the $n = \frac{3}{2}$ and $n = 3$ were small. Further, there is a total mass difference of 25 per cent derived from different sides of M31. This reflects the surprising differences between the rotation-curves derived for each side of M31 and illustrated in Figure 5. The sense of these differences are similar to those found by BTT (1964*a*) and derived by a completely different method: model fitting to velocity profiles.

Adopting the $n = \frac{3}{2}$ combined-data solution giving the best fit, we find for the total mass of M31

$$\mathfrak{M}_{\text{total}} = 3.1 \pm 0.5 \times 10^{11} \odot ,$$

where the uncertainty is estimated from the results of the other solutions in Table 3. This value is also the average of the masses computed for the two halves separately.

If we assume that the three most distant points on each side of the rotation-curve are in Keplerian motion, we can make the following mass estimates: NF, $\langle R \rangle = 22.7$ kpc, $\mathfrak{M} = 2.9 \times 10^{11} \odot$; SP, $\langle R \rangle = 20.8$ kpc, $\mathfrak{M} = 1.6 \times 10^{11}$. These values are significantly

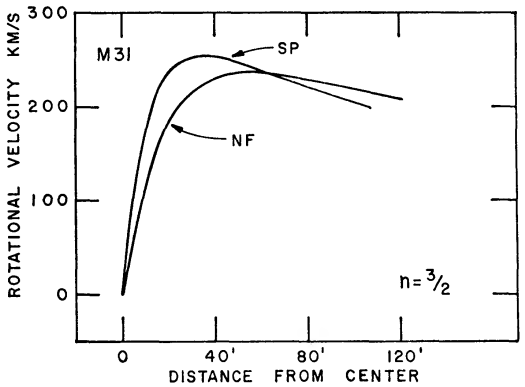

FIG. 5.—A comparison of the rotation-curves derived from each side of M31

lower than any of the masses in Table 3, but their difference is in the same sense as found from the complete solution for either the $n = \frac{3}{2}$ or $n = 3$ cases. The fact that they are low shows how poor our assumption of Keplerian motion was, even at distances of $\sim$20 kpc from the nucleus. That one has not reached the Keplerian region of the rotation-curve even well beyond the turnover point is clearly evident in the model calculations of Toomre (1963, Fig. 1).

Various parameters of the total mass distribution may be derived from a rotation law of the form given in equation (3); the necessary relations and tabular material for such an analysis have been summarized by Brandt and Scheer (1965). In this manner we have derived a central density of 1.2×10^{-22} gm/cm^3, assuming an axial ratio $c/a = 0.1$. The projected surface density, Σ_{total}, at $R = 10$ kpc, the location of the hydrogen ring in M31 discussed below, is 0.034 gm/cm^2 = 162 $\odot$/pc^2.

As can be seen in Figure 4, the optically derived points for the rotation-curve deviate from the least-squares solution for the 21-cm data. That a discrepancy between the optical and 21-cm solutions exists was first noted by van de Hulst *et al.* (1957). They found that the optical points lay above both halves of the 21-cm rotation-curve by $\sim$100 km/sec, the same as shown in Figure 4. We see in this figure that there is better qualitative agreement between the complex-region points and the optical data. An examination of Figure 1 in Mayall's (1951) paper shows that his measures out to 1° radius were confined exclusively to the two complex quadrants. There is thus some semblance

of agreement between the radio and optical data when they both refer to the same regions of Andromeda. Mayall (1965) has cautioned against an overevaluation of his data since he feels that they are of low precision and may have large systematic errors. Additional optical observations are obviously necessary before a general agreement between the complex-quadrant radio and optical data can be accepted.

c) *The Systemic Radial Velocity*

The method employed in deriving the systemic radial velocity has been described in the previous section. As an example illustrating the procedure we compare the combined-data solutions for two values of s. For the $n = \frac{3}{2}$ case, $s = -310$ km/sec gives an rms

TABLE 4

MEASURES OF THE SYSTEMIC RADIAL VELOCITY OF M31

Source	Radial Vel. (km/sec)	Remarks
Optical:		
Slipher	−300	From compilation by H. W. Babcock (1939), references given therein
Wolf	−350	
Wright	−304	
Pease	−316	
Pease and Adams (I)	−329	
Pease and Adams (II)	−297	
Humason	−220	
Babcock (1939)	−300	Estimated from rotation-curve
Humason	−266±15 (est. error)	From 2 spectra (Humason, Mayall, and Sandage 1956)
Mayall	−290	From 7 spectra, residuals range from +49 to −38 km/sec (Humason *et al.* 1956)
21 cm:		
Van de Hulst *et al.* (1957)	−300±3 (mean error)	From reflecting velocity profiles at symmetric points of major axis
Argyle (1965)	−299 6±0 4	The radial velocity of the centroid of the hydrogen distribution
BTT (1963)	−302	Symmetry points of rotation-curve for major-axis observation
	−314--324	From symmetry of minor-axis observation
This study	−310±3 (est. error)	See text

of the residuals of 24.2 km/sec; for $s = -300$ the rms residual is 36.1 km/sec; for the $n = 3$ case, $s = -310$ gives a residual of 25.8 km/sec and the $s = -300$ solution gives a residual of 36.7 km/sec. Thus, the rms of the residuals are about 50 per cent larger for the $s = -300$ case than for the $s = -310$ case. As noted earlier, a value of $s = -310 \pm 3$ km/sec was adopted.

A summary of various determinations, both optical and 21 cm, of the systemic radial velocity of M31 is given in Table 4. The first seven optical determinations are from a compilation by Babcock (1939); the original source references are given there. All of the optical measures except Babcock's own value refer to the bright nuclear region of M31. Babcock's value is based on radial-velocity measures of the nuclear region as well as on the general appearance of the rotation-curve derived from measures along the major and minor axes.

A brief description of the method used in the 21-cm determination is given in the "Remarks" column of Table 4. The small error in the value given by Argyle reflects

internal scatter only. Since he gives the radial velocity of the center of mass of the H I system, a difference between this value and the true systemic velocity could exist if the hydrogen distribution is not symmetric with respect to the rotation axis of M31. This general question has been considered previously (Roberts 1965).

The unweighted average of the optical determinations of s is -297 ± 11 (standard error) km/sec. Omitting Humason's early value, we obtain $s = -306 \pm 8$ (standard error) km/sec. In view of the varying weights and unknown systematic errors in these measures, we conclude that there is no significant difference between the optical and 21-cm determinations of the radial velocity of M31.

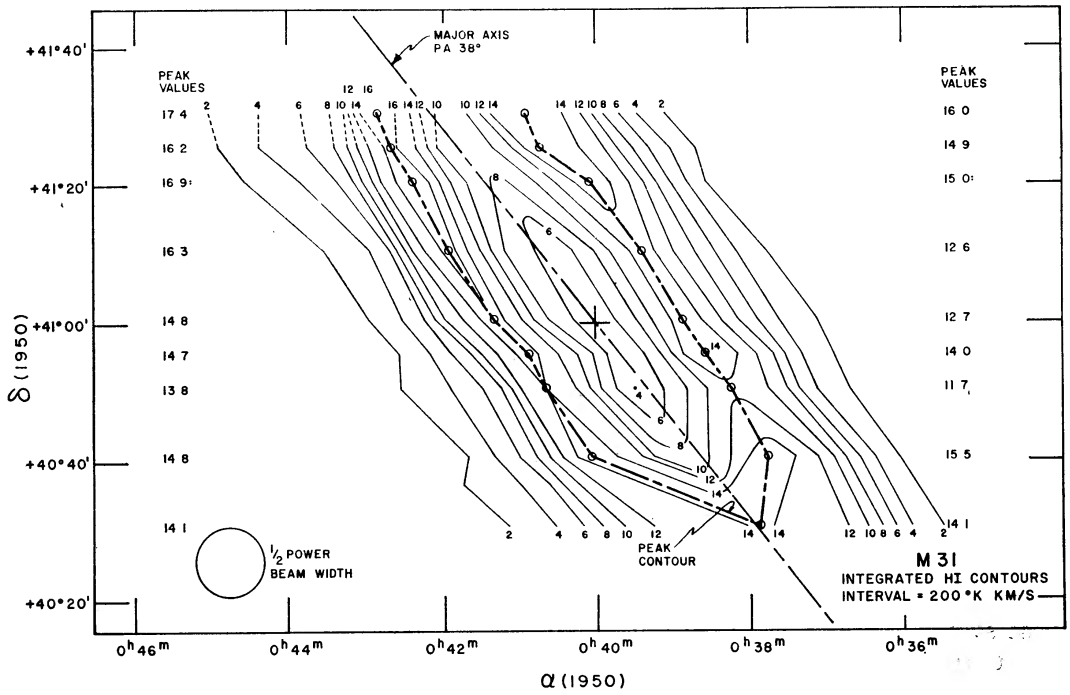

FIG. 6.—Contours of equal integrated brightness temperature. The individual contour levels are in units of 100° K × km/sec. The peak ridge level is indicated as a heavy dashed line and is defined by the small open circles whose values are listed on each side of the figure. No correction for beam-smearing has been made.

d) Integrated Hydrogen Distribution

A contour map of the integrated (summed over all velocities) brightness temperature as seen by the 10′ beam of the 300-foot telescope is presented in Figure 6. This map refers only to those regions which have a complete velocity coverage. The peak contour level is indicated as a heavy dashed line and is defined by the small circles along this line. The values of the peak brightness temperature for each of the circles is given in the columns on each side of the map. The data represent observations at nine different declinations taken over the two observing periods, with several of the declinations common to both observing periods. The brightness-temperature scale is believed to be accurate to better than 10 per cent, but some of the individual peak values may be in error by as much as 20 per cent. The locations of the peak values should be significantly more accurate than the positional data for individual drift-curves discussed earlier.

The relation of the hydrogen contours to the optical image of M31 is shown in Figure 7; the photograph is from the blue print of the 48-inch Schmidt Sky Survey Atlas. The image of Andromeda on the survey print extends beyond the limits of Figure 7, and it is these extensions that define the major axis.

If the hydrogen is optically thin, then these contour lines display the distribution of neutral atomic hydrogen as seen on the projected image of M31. The striking feature in this distribution is the concentration of hydrogen on each side of the galaxy. These maximum ridge lines join at the SP end of the map resulting in an elliptical contour similar in outline to the projected image of M31. This maximum ridge line, when projected into the plane of the galaxy, indicates that the hydrogen (over the surveyed region) is concentrated in a ring 10 kpc in radius, as measured along the minor axis, assuming an inclination of 77°. The closing of the ring at the SP end is defined by a broad, velocity integrated, drift-curve, and may only be due to a local concentration of H I, perhaps related to the prominent emission nebula (Mount Wilson No. 22, SP end) situated close to the SP peak value on the major axis (see Fig. 7). The BTT survey along the major axis shows that concentrations of hydrogen will also be found at ~62′ (SP), 49′ (NF), and ~67′ (NF).

The integrated brightness contours of Figure 6 may be converted to projected densities perpendicular to the plane by means of the following relation:

$$N_{\mathrm{H\,I}} = 5.94 \times 10^{-4} \cos \xi \int_{-\infty}^{+\infty} T_B dv\,, \tag{5}$$

where $N_{\mathrm{H\,I}}$ is the number of neutral atomic hydrogen atoms/cm^3 kpc^{-1}, T_B is the brightness temperature averaged over the beam, and the integration is over all velocities in km/sec. Thus, for the peak integrated brightness value in Figure 6 of 17.4×10^2 ° K km/sec, $N_{\mathrm{H\,I}}$ is 0.23 atoms/cm^3 kpc^{-1}. Along the major axis at 38′ SP, the projected density is 0.19 atoms/cm^3 kpc^{-1} in good agreement with the value of 0.16 obtained by BTT through model fitting to the velocity profiles. The average peak brightness temperature along that part of the ring measured here is 1480° K/km/sec corresponding to 0.20 atoms/cm^{-3} kpc^{-1} = 1.02×10^{-3} gm^{-1} cm^{-2} = 4.88 $\odot$/pc^2. The ratio $\Sigma_{\mathrm{H\,I}}/\Sigma_{\mathrm{total}}$ at R = 10 kpc is 3.0 per cent.

In Figure 7 we see the relation of M32 (*lower left*) and NGC 205 (*upper right*) to the hydrogen contours. No anomalies in the observed contours are apparent near either of these systems. For NGC 205 the contour levels below those plotted, 200 ° K/km/sec, were examined but no obvious features was noted.

A comparison between the 21-cm brightness distribution and the optical distribution of emission nebulae is shown in Figure 8. For the latter we have used a reproduction of the map constructed by Baade and Arp (1964, Fig. 1). Figure 8 shows the individual emission nebulae as small filled circles as well as the set of curved lines illustrating Baade's preliminary interpretation of the organization of the emission nebulae into spiral arms. The details of the H I contours of Figure 6 have been retained in the composite of Figure 8, with the addition of two heavy arrows to assist in locating the peak H I contours, which appear as heavy dashed lines. The diagonally placed scales on either side have been retained from the Baade-Arp figure; each division corresponds to 10′.

The outstanding feature in this comparison is the excellent agreement of the general run of the peak H I contour with the concentrations of H II regions—the optically defined spiral arms. The large concentrations of emission regions in the upper left of the diagram (NF end, east side) also has the highest integrated brightness temperatures. However, the detailed fit of the H I peak ridge line to the emission regions differs by 0.′5 to 1.′5 with an average difference of about 1′ in the sense that H I ridge lines lie west of the optical concentrations. An angular distance of 1′ corresponds to 200 pc on the plane of the sky, and to 200 (sec ξ) = 0.9 kpc in the plane of the galaxy. Thus, this difference becomes quite significant for the question of the coincidence of optical spiral features and H I "arms." The estimated *maximum* error in the absolute pointing of the 300-foot telescope at this declination in right ascension and declination combined is 0.′9. Only by invoking this maximum pointing error can we attribute the displacement of the optical

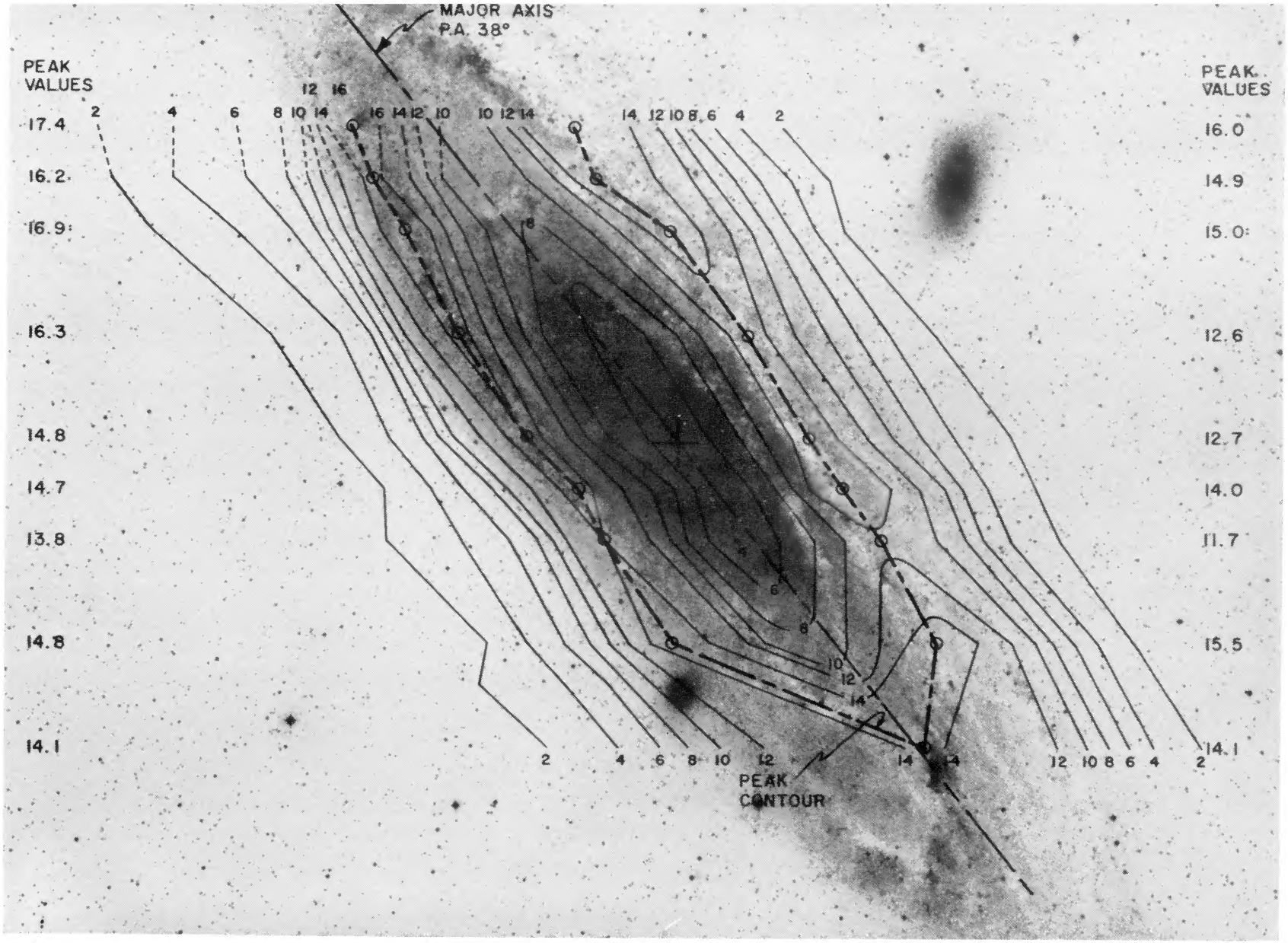

FIG. 7.—The integrated brightness-temperature contours of Fig. 6 superposed on a blue photograph of M31. The general placing of the "ring" of H I is in a dust lane on the west side and near concentrations of emission regions on the east. The major axis is defined by outer regions lying beyond the limits of the photograph. (M31 photograph from the 48-inch Palomar Schmidt Sky Survey Atlas.)

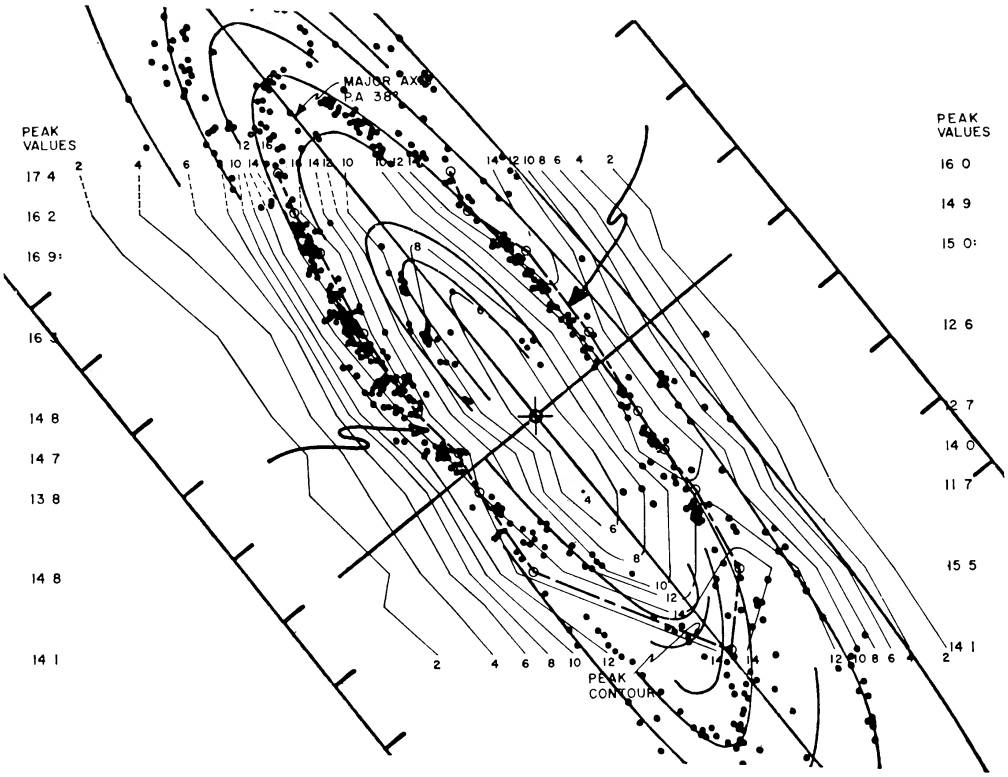

FIG 8.—Comparison of the 21-cm brightness-temperature contours of Fig. 6 and the distribution of emission nebulae as mapped by Baade and Arp (1964). The two heavy arrows indicate the peak H I ridge lines.

TABLE 5

SUMMARY OF PARAMETERS ADOPTED OR DERIVED FOR M31

Distance	0.69 Mpc
Systemic radial velocity (km/sec)	
21 cm:	-310 ± 3 (est. error)
Optical:	-297 ± 11 (standard error)
Position angle	38°
Inclination	77°
Estimated maximum inclination for bends	85°
A (see equation (3), $n = \frac{3}{2}$)	2.67×10^{-15} sec^{-1}
B (see equation (3), $n = \frac{3}{2}$)	5.77×10^{-23} cm^{-1}
Maximum circular velocity	244 km/sec
Location of maximum circular velocity	8.9 kpc
Total mass, $\mathfrak{M}_T$	$3.1 \pm 0.5 \times 10^{11}$ ⊙
Diameter of H I ring	10 kpc
$\mathfrak{M}_{H\,I}$	3.68×10^{9} ⊙
$\mathfrak{M}_{H\,I}/\mathfrak{M}_T$	1.2 per cent
$(M_{pg})_0$	−21.1
$\mathfrak{M}_{H\,I}/L_{pg}$	0.095
Central density ($c/a = 0.1$ adopted)	1.2×10^{-22} gm/cm^3
Surface density, Σ_T, at $R = 10$ kpc	0.034 gm/cm^2 = 162 ⊙/pc^2
Average H I surface density $\Sigma_{H\,I}$ at $R = 10$ kpc	1.02×10^3 gm/cm^2 = 4.9 ⊙/pc^2
$\Sigma_{H\,I}/\Sigma_T$ at $R = 10$ kpc	3 per cent

arms and peak hydrogen contours to instrumental effects. There is thus a significant probability that the observed displacement is real and may be as large as 1 kpc. A similar lack of coincidence between optical and 21-cm arms has been suggested for our own Galaxy (e.g., Becker 1960, Muhleman and Walker 1964).

Adjusting Argyle's (1965) value of the total H I content of Andromeda to the distance adopted here, we obtain $\mathfrak{M}_{\mathrm{H\,I}} = 3.68 \times 10^9\ \odot$; this gives a hydrogen to total mass ratio of 1.2 per cent. For an absolute magnitude of $(M_{\mathrm{pg}})_0 = -21.1$ (Chester and Roberts 1964), which includes a correction to a face-on orientation, we obtain 0.095 for the distance-independent quantity $\mathfrak{M}_{\mathrm{H\,I}}/L_{\mathrm{pg}}$. These values together with the various other parameters adopted or derived in this study are summarized in Table 5.

In summary, we conclude (1) that the principal plane of the hydrogen distribution in M31 is bent at either end in a manner similar to that found in our own Galaxy; (2) ordered, non-circular motions occur over a scale of kiloparsecs with some regions moving outward and others inward; (3) the rotation-curve is not symmetric about the center; (4) over the region surveyed, the principal hydrogen distribution is ring-shaped; (5) there is good general agreement between the location of optically observed H II emission regions and the peak H I contour. However, the small difference that does exist may be real and would then indicate a difference of up to 1 kpc between the optical and H I features.

I would like to thank Kurtiss Gordon and Nancy Remage for assistance in the preparation and reduction of the extensive data.

REFERENCES

Argyle, E. 1965, *Ap. J.*, **141**, 750.
Arp, H. 1964, *Ap. J.*, **139**, 1045.
Baade, W., and Arp, H. 1964, *Ap. J.*, **139**, 1027.
Baade, W., and Swope, H. H. 1963, *A.J.*, **68**, 435.
Babcock, H. W. 1939, *Lick Obs. Bull.*, **19**, 41.
Becker, W. 1960, *Z. f. Ap.*, **51**, 152.
Brandt, J. C. 1960, *Ap. J.*, **131**, 293.
Brandt, J. C , and Scheer, L. S. 1965, *A.J.*, **70**, 471.
Brundage, W. D., and Kraus, J. D. 1965, *A.J.*, **70**, 669.
Burke, B. F. 1957, *A.J.*, **62**, 90.
Burke, B. F., Turner, K. C., and Tuve, M. A. 1963, *Annual Report of the Director, Dept. of Terrestrial Magnetism, 1962–1963* (Washington, D.C.: Carnegie Institution of Washington), p. 289.
———. 1964*a*, *Annual Report of the Director, Dept. of Terrestrial Magnetism, 1963–1964* (Washington, D C.: Carnegie Institution of Washington), p. 341.
———. 1964*b*, *The Galaxy and the Magellanic Clouds*, ed. F. J. Kerr and A. W. Rodgers (I.A.U.-URSI Symp. No. 20; Canberra: Australian Academy of Sciences), p. 131.
Chester, C., and Roberts, M. S. 1964, *A.J.*, **69**, 635.
Gum, C. S., Kerr, F. J., and Westerhout, G. 1960, *M.N.*, **121**, 132.
Höglund, B , and Roberts, M. S. 1965, *Ap. J.*, **142**, 1366.
Hulst, H. C. van de, Raimond, E., and Woerden, H. van. 1957, *B.A.N.*, **14**, 1.
Humason, M. L., Mayall, N. U., and Sandage, A. R. 1956, *A.J.*, **61**, 97.
Kahn, F. D., and Woltjer, L. 1959, *Ap. J.*, **130**, 705.
Kerr, F. J., Hindman, J. V., and Carpenter, M. S. 1957, *Nature*, **180**, 677.
Lohman, W. 1954, *Z. f. Ap.*, **35**, 159.
Lynden-Bell, D. 1965, *M.N.*, **129**, 299.
Mayall, N. U. 1951, *Pub. Observatory Univ. of Michigan*, **10**, 19.
———. 1965 (private communication).
Muhleman, D. O., and Walker, R. G. 1964, *A.J.*, **69**, 95.
Oort, J. H. 1965, *Transactions I.A.U.*, **12A** (New York: Academic Press), 789.
Roberts, M. S. 1965, *Ap. J.*, **142**, 148.
Robinson, B. J. 1965, *Symposium on the Magellanic Clouds*, ed. J. V. Hindman and B. E. Westerlund (Mount Stromlo Observatory), p. 6.
Schwarzschild, M. 1954, *A.J.*, **59**, 273.
Toomre, A. 1963, *Ap. J* , **138**, 385.
Vaucouleurs, G. de. 1958, *Ap. J.*, **128**, 465.